J. Fluid Mech. (1991), *vol.* 229, *pp.* 1–27
Printed in Great Britain

Fluid skimming and particle entrainment into a small circular side pore

By ZONG-YI YAN[1]†, ANDREAS ACRIVOS[1] AND SHELDON WEINBAUM[2]

[1] The Levich Institute, The City College of The City University of New York, New York, NY 10031, USA

[2] Department of Mechanical Engineering, The City College of The City University of New York, New York, NY 10031, USA

(Received 13 February 1990 and in revised form 26 November 1990)

It is a well-known observation in fluidization technology, axial filters and the blood microcirculation that the discharge concentration of a particulate suspension through a small circular side pore which is fed by a large main tube can be significantly lower than the feed concentration. Two underlying mechanisms are believed to be responsible for this exit concentration defect: the fluid skimming from the particle-free layer at the main tube wall and the particle screening due to the hydrodynamic interaction with the pore entrance. In this paper we shall focus our attention only on the first mechanism and shall present a theory which relates the discharge concentration to the dimensionless volume discharge rate $2\pi Q$ through the side pore (scaled to the wall shear rate in the main tube and the pore radius) and the ratio of the particle to pore entrance diameters, under creeping flow conditions and for small particle concentrations. First, the shape of the capture tube cross-section upstream of the pore is computed on the basis of a simplified three-dimensional velocity field which neglects the disturbance produced by the orifice on the incoming shear flow. Surprisingly simple closed-form expressions for this shape are derived as $Q \to \infty$ or as $Q \to 0$. Also, using a recently developed exact solution for the simple shear flow past an orifice (Davis 1991), we are able to rigorously demonstrate that, even for small Q, the disturbance produced by the orifice on the shear flow has only a minor effect on the capture tube cross-section far upstream. This simplified flow field is then used to construct a three-dimensional theory for the discharge concentration defect due to pure fluid skimming for a dilute suspension of spheres. The qualitative features of the theoretical predictions show the same trends as the experimental observations in the microcirculation, although the limits of this theory are well below the observed hematocrit concentrations and the particles are taken as rigid spheres.

1. Introduction

The problem of particle entrainment from a shear layer flowing past a solid boundary containing small pores has important application in fluidization technology, axial flow filters and the microcirculatory behaviour involving the distribution of the cellular components of blood. The primary motivation for the

† On leave from Department of Mechanics, Peking University, Beijing, PR China 100871.

present study was the well-known observation (Cokelet 1976; Chien, Usami & Skalak 1984; Gaehtgens & Papenfuss 1979; Lipowsky 1986; Pries, Ley & Gaehtgens 1986) that, in microvessels having diameters smaller than approximately 30 μm, the discharge hematocrit H_D (volume fraction of red cells in a plasma suspension) could be significantly less than the feed reservoir hematocrit H_F and could vary substantially with the shear flow rate. This behaviour has been attributed to two phenomena: (i) *plasma skimming* from the cell-free layer at the wall of the feeding vessel and (ii) *particle screening* due to the hydrodynamic interaction of the cells with the pore entrance geometry. These same phenomena occur more generally in a host of other applications where a suspension flowing under shear is being drained at a solid boundary with pores. Apparently though, no theoretical framework at present exists for elucidating quantitatively how the discharge concentration H_D through the pores is related to the local shear in the upstream boundary layer, the volume discharge through the pore and the ratio of the particle diameter to that of the pore entrance. In this paper a simplified three-dimensional theory will first be developed to describe the fluid capture tube upstream of the pore and this theory will then be applied to determine the discharge hematocrit defect of a dilute suspension of rigid spheres due to pure fluid skimming. Although the limits of this theory are below the hematocrit concentrations (10 to 40%) observed in the microcirculation, the qualitative features of the theoretical predictions show the same trends as the experimental measurements. The additional contribution to the discharge hematocrit defect due to mechanism (ii), particle screening, will be examined in a companion study (Wu, Weinbaum & Acrivos 1991).

In the applications mentioned above one is largely interested in the entrainment of particles of one to several tens of microns through pores of comparable dimensions, and hence, under these conditions, gravity is negligible compared to the hydrodynamic forces on the particles. Suppose then that the average fluid velocity in the main tube is U, the ratio of the pore radius c to the main tube radius b is β with $\beta \ll 1$, and that the non-dimensional volumetric fluid flux into the pore is $2\pi Q$ (scaled with the wall shear rate in the main tube and the pore radius c). Then, we shall show through an asymptotic analysis that, if the velocity at a distance c from the main tube wall is of $O(\beta U)$, and the average velocity in the pore is of $O(\beta UQ)$, the height of the upstream capture tube will be $O(Q^{\frac{1}{3}}c)$ if $Q > 1$. In the microcirculation Q will typically lie in the range $0 < Q < 0.2$, and in other applications Q could be as large as $O(10)$ or more. Thus, for $Q > 1$, the velocity of the shear flow at the top of the capture tube will be $O(Q^{\frac{1}{3}}\beta U)$ and the Reynolds number describing the flow in the capture tube will be $O(Q^{\frac{2}{3}}\beta^2 Re_b)$ where Re_b is the Reynolds number in the feed tube. Similarly, the Reynolds number for the flow through the pore will be $O(Q\beta^2 Re_b)$. Thus, if $\beta \ll 1$, the particle entrainment problem can be treated as a Stokes flow problem even if Q is of $O(10)$ and the Reynolds number of the main tube flow is large compared to unity. In the microcirculation $Re_b \ll 1$ and this restriction on β is not required.

The Stokes flow approximation is an important simplification in that it enables us to treat the rather complicated three-dimensional flow geometry shown in figure 1 as the superposition of two simpler flows: (i) the axisymmetric suction flow from an otherwise quiescent half-space into a pore and (ii) the linear shear flow past the pore without suction. An infinite series solution to problem (i) was presented in Dagan, Weinbaum & Pfeffer (1982), who considered the more general case of the flow between two infinite half-spaces connected by a finite-length pore. Two important simplifying features of this solution were (*a*) that the solutions in the half-space could

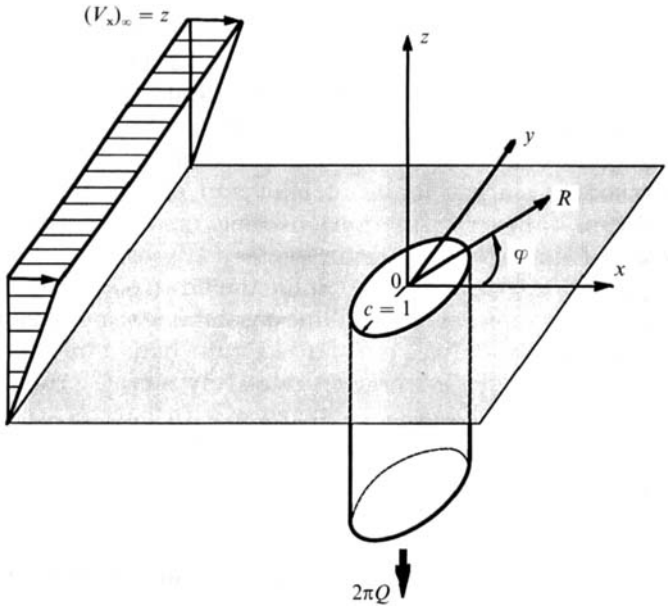

FIGURE 1. Geometry.

be accurately approximated by Sampson's solution (Sampson 1891; Happel & Brenner 1973) for the flow through a circular orifice in a plane wall except for the immediate vicinity of the orifice opening, and (*b*) that, if the pore length were more than half the pore radius, the axial velocity profile in the plane of the opening could be approximated to four digits by the arithmetic mean of a Poiseuille and a Sampson profile. Problem (ii), which is the axisymmetric analogue of Takematsu's (1966) two-dimensional solution for the shear flow past a slot in a plane wall, has recently been considered by Tutty (1988) as part of an accurate and detailed numerical solution for the shear flow past a long side-branch tube with suction. An important simplification noted in problem (ii) is that the perturbation to the simple shear flow in the half-space is very small except in the immediate vicinity of the pore entrance, where the dividing streamline penetrates a small fraction of the pore radius into the side branch. Of course, if the slot were infinitely long, one would obtain an infinite sequence of decaying countercurrent eddies of equal aspect ratio (Moffatt 1964). The equivalent problem for the linear shear flow past an orifice in a plane wall has recently been solved by Davis (1991). This solution will be used herein to show that although the transverse velocity disturbance due to the shear at the orifice entrance does not vanish as $Q \to 0$, its effect on the capture tube cross-sections far upstream is slight in the limit of small Q and therefore can be ignored for all Q.

Tutty's combined numerical solutions to problems (i) and (ii) above are much too laborious to easily use in the present study where the primary interest lies in determining the three-dimensional shape of the capture tube streamlines and the phase separation of the particles as they approach the pore entrance. Tutty's solutions, however, provide a valuable standard by which the accuracy of the approximations used in the present study can be assessed and also suggest certain simplifying features for treating the combined problem. For example, these solutions indicate that the counter-rotating vortices in problem (ii) are much weaker than their two-dimensional counterparts and will be washed out of the side-branch tube

entirely at very small suction velocities ($Q \geqslant 0.027$). This critical value of Q for the disappearance of the side-branch vortices is significantly smaller than the physiological range for Q in the microcirculation cited earlier. As expected, it is found that the capture tube streamlines at upstream infinity form a two-dimensional cylinder whose cross-sectional shape depends on Q. Although, in general, the geometry of this cross-section is rather complicated, it will be shown via an asymptotic analysis that, in the limits of high and of low Q, the shapes of the corresponding capture tube cross-sections assume distinct forms which can be described by means of simple analytic expressions.

In §2 we shall propose a simple expression for the flow treated by Tutty (1988) in which the fluid velocity is represented as a linear combination of a simple shear flow and a Sampson flow. The streamlines and capture tube boundaries for the fluid were then calculated by numerically integrating relatively simple ordinary differential equations in three dimensions. Even so, comparison with Tutty's accurate numerical solution shows that this much simpler velocity profile leads to streamline shapes and upstream capture tube geometries which agree remarkably well with the exact solution except in the immediate vicinity of the pore entrance. Furthermore, for the two limiting cases of very small or very large side-branch fluxes, the differential equations can be integrated analytically to provide closed-form expressions for the asymptotic far-field streamlines and entrainment tube shapes in the upstream shear flow. In turn, these approximate asymptotic solutions in §3 lead to a greatly simplified analysis of the plasma skimming effect, which is examined in §4.

The most important limitation of this simplified model for the basic flow is that it neglects the transverse velocity at the mouth of a pore of finite length. Yet it is known from the analysis of Sobey (1977) and of Tutty (1988) that the deviation of the local wall shear in the main tube from that exerted by the linear flow depends only on this transverse velocity component, in contrast to the wall pressure distribution, which is related only to the normal velocity component at the pore opening. Thus, for a Sampson flow in which the transverse velocity component at the pore opening vanishes, the dividing streamline for the capture tube must attach to the wall at the edge of the pore. Although such a non-zero transverse velocity has little influence on the geometry of the upstream capture tube, it does affect the locus of the attachment boundary defined by the contours of zero wall shear stress in the main flow direction. The numerical solutions in Tutty's paper show, however, that attachment occurs very close to the edge provided Q is of $O(1)$ or smaller. For larger values of Q we shall derive in §5 a simple closed-form expression for the wall shear distribution in the vicinity of the pore entrance, which can be conveniently used to predict the attachment boundary contours without the need of numerical procedures. Such contours are of special interest in exploring the relationship between the topological distribution of the wall shear stress and the localization of atherosclerotic lesions in the vicinity of the entrance of the arterial branches of the aorta as observed by Cornhill & Roach (1976) and discussed by Tutty (1988).

A brief discussion of the qualitative features of plasma skimming as they relate to the defect in the discharge hematocrit H_D is given in §6; while a more detailed presentation of the biological applications of this study is presented in Yan, Acrivos & Weinbaum (1991).

2. Simplified model for the fluid streamlines and the fluid capture tube

We wish to construct a simplified mathematical description for the velocity in the flow geometry depicted in figure 1, which is representative of a channel flow with non-interacting pores, an axial flow filter, or a tube flow where the radius b of the feeding vessel is large compared to the radius c of the circular orifice or side branch so that the curvature of the former may be neglected. The origin of the coordinate system is taken at the centre of the pore opening and the z-axis points upward along the pore axis (figure 1). Cartesian (x, y, z) and cylindrical coordinates (R, φ, z) will be used alternatively for mathematical convenience. The flow along the wall far from the pore opening consists of a simple shear flow in the x-direction whose shear rate is taken as unity. All other quantities are non-dimensionalized with respect to this shear rate and the pore radius and, if the dimensional volume flow through the side branch is of $O(Qc^2\beta U)$, then, as shown in the introduction, the Stokes flow equations will be valid throughout the flow region of interest, even if $Q \gg 1$, as long as the Reynolds number in the capture tube, which is $O(Q^{\frac{2}{3}}\beta^2 Re_b)$, is $\ll 1$. Moreover, since according to the solution in Dagan *et al.* (1982), the streamlines for the axisymmetric Stokes flow into the pore differ from those of a Sampson flow through a circular orifice only in the immediate vicinity of the pore opening and since Tutty's (1988) solution for a simple shear flow past a circular pore with no suction produces only a very weak counter-rotating vortex flow within the side branch, it seems reasonable to expect that, to a good approximation, the velocity field could be represented as a superposition of a Sampson flow and a simple shear flow. This superposition should describe the flow accurately everywhere within the upper half-space, even in the limit $Q \ll 1$, as will be shown in §3.3. This simplified velocity field, with the Sampson flow denoted by the superscript s, is given by

$$V_x = z + \frac{x}{R} V_R^{\mathrm{s}}, \quad V_y = \frac{y}{R} V_R^{\mathrm{s}}, \quad V_z = V_z^{\mathrm{s}}, \tag{1}$$

where

$$V_R^{\mathrm{s}} = \tfrac{3}{4} Q z \frac{\zeta}{R} (R_1 - R_2)\left(\frac{1}{R_1} - \frac{1}{R_2}\right), \quad V_z^{\mathrm{s}} = -\tfrac{3}{4} Q \frac{\zeta}{R} (R_1 - R_2)\left(\frac{R-1}{R_1} - \frac{R+1}{R_2}\right), \tag{2}$$

with $2\pi Q$ being the volumetric fluid flux into the pore, and

$$R = (x^2 + y^2)^{\frac{1}{2}}, \quad \zeta = [1 - \tfrac{1}{4}(R_2 - R_1)^2]^{\frac{1}{2}},$$

$$R_1 = [z^2 + (R-1)^2]^{\frac{1}{2}}, \quad R_2 = [z^2 + (R+1)^2]^{\frac{1}{2}}.$$

In addition, the fluid streamlines satisfy

$$\frac{\mathrm{d}x}{\mathrm{d}s} = \frac{V_x}{V}, \quad \frac{\mathrm{d}y}{\mathrm{d}s} = \frac{V_y}{V}, \quad \frac{\mathrm{d}z}{\mathrm{d}s} = \frac{V_z}{V}, \tag{3}$$

where $V = (V_x^2 + V_y^2 + V_z^2)^{\frac{1}{2}}$ and s is the arclength along the streamline. Although the streamline equations (3) are too difficult to integrate analytically for the general case, we shall see in the next section that closed-form analytic results can be obtained for the limiting cases where Q is either very large or very small.

Of special interest are the dividing streamlines. For the flow represented by (1) these streamlines must terminate at the pore edge, $z = 0$ and $R = 1$, since the

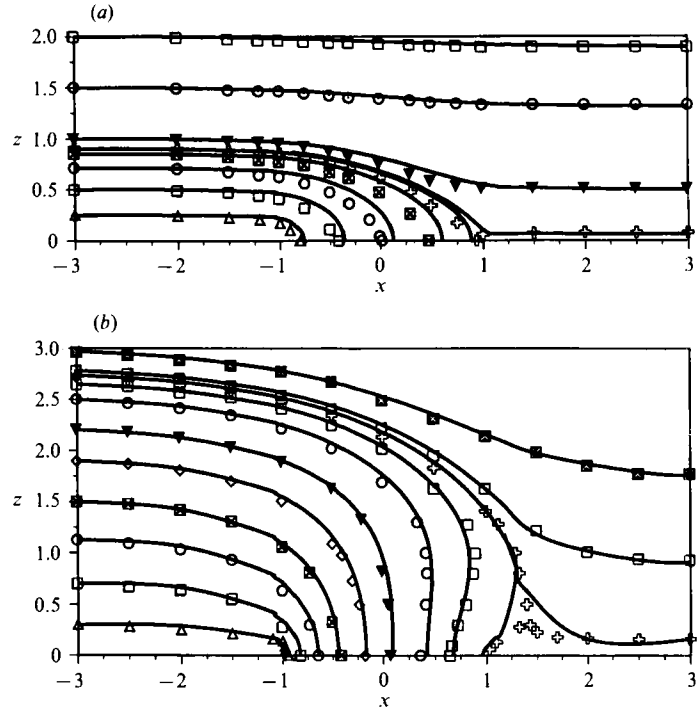

FIGURE 2. Comparison of the streamlines in the $y = 0$ plane (solid lines, our simplified model using (2) and (3); symbols, Tutty 1988): (*a*) $Q = 0.11$; (*b*) $Q = 2$.

Sampson flow is symmetric about the plane $z = 0$ and thus cannot produce a wall shear to negate that of the incoming simple shear flow ($V_x = z$). These streamlines form a fluid capture tube within which the fluid phase is sucked into the pore. To find the upstream shape of this capture tube for an arbitrary value of Q, (3) was integrated numerically along the dividing streamline starting from the pore edge using a fourth-order Runge–Kutta technique. In practice, the numerical integration procedure was begun at a negligible distance from the exact edge, $z = 0$ and $R = 1$, to avoid the singularity in the flow field at this point. Numerical tests showed that this manoeuvre produced no perceptible errors in the capture tube shape. To obtain the desired accuracy, the step lengths were varied from 10^{-5} in the vicinity of the pore edge to 10^{-2} in the region far upstream. This provided an upstream capture tube cross-section which was accurate at least to order 10^{-4}.

The numerical integrations just described were performed for values of Q in the range of 10^{-3} to 10^{3}. Figure 2 shows the streamline patterns in the symmetry plane $y = 0$ for $Q = 0.11$ and 2.0, where it should be noted that $Q = 0.11$ lies in the middle of the physiological range of this parameter in the microcirculation. Also plotted in this figure are Tutty's exact numerical results. One observes that, at $Q = 2$, the two streamline patterns are nearly identical everywhere except near the downstream attachment point where, according to the exact solution, the flow attaches to the wall a short distance downstream of the edge. For larger values of Q which are not shown, this attachment point moves further downstream and the deviation from the exact solution will become larger. In §5 an approximate theory will be presented to determine the attachment point on the downstream wall for these larger values of Q. On the other hand, for $Q = 0.11$ larger deviations in the streamline behaviour are

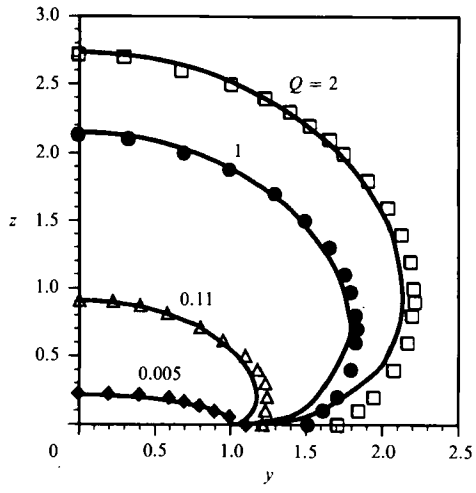

FIGURE 3. Comparison of our fluid capture tube cross-section shapes at $x = -3$ (solid lines) with Tutty's results (symbols).

observed directly over the pore, but on either side of the pore and within the symmetry plane the streamlines of our approximate model and those of the exact solution are nearly indistinguishable.

In figure 3 the capture tube cross-sections at an upstream location ($x = -3$) are compared with Tutty's exact numerical solutions. Again, the agreement is almost perfect except for the location of the wall attachment point. This discrepancy again arises from the fact that a Sampson flow does not generate a transverse velocity in the plane of the pore opening and thus gives rise to an inaccurate upstream attachment point. A surprising observation is that even for the smallest value of Q shown, 0.005, the upstream capture tube shapes as obtained from the two solutions are in remarkably good agreement even though, for this value of Q, the exact solution (see Tutty's figure 5) shows that a large primary vortex exists in the side-branch pore and that the normal velocity profile deviates significantly from the Sampson solution. This good agreement will be explained in the next section using an asymptotic analysis that is valid for $Q \ll 1$.

We further wish to note that the capture tube cross-sections in figure 3 illustrate two fundamentally different shapes for $Q > 2$ and $Q \ll 1$. Specifically, in the low-Q limit, the tubes are nearly two-dimensional elliptic cylinders whose width is nearly the same as the pore diameter, whereas, for the large values of Q, the cross-section extends far beyond the boundaries of the pore. The asymptotic analysis in the next section will provide additional insight into this intriguing difference.

3. Asymptotic solutions

Although the complicated form of the velocity field, as given by (2), precludes the analytical determination of the streamlines and in particular of the shape of the capture tube at upstream infinity for arbitrary Q, it is possible to derive closed-form expressions for these quantities when Q is very large or very small. In fact, we shall show that the capture tubes thereby obtained are in very close agreement with those computed via our simplified numerical solutions in §2 as well as with Tutty's finite-difference solutions except for a relatively narrow intermediate range in Q which lies

roughly between 0.1 and 1.0. Specifically, we shall derive in §3.1, the asymptotic solution for $Q \gg 1$ using a superposition that consists of a linear shear flow and a Stokes sink in a half-space, while, in §3.2 we shall examine the $Q \ll 1$ limit using a superposition of a linear shear flow, which neglects the disturbance velocity in the x-direction over the hole, and a Sampson flow through the hole (i.e. the same simplified profile considered in §2). But, since for $Q \ll 1$, this approximation appears questionable in view of the fact that the disturbance velocity produced by the shear flow past the orifice opening becomes of comparable magnitude with the Sampson flow as the plane $z = 0$ is approached, we shall undertake in §3.3 a more rigorous analysis in which the recently derived exact solution of Davis (1991) for the shear flow past an orifice is used to analyse the capture tube boundary in the vicinity of the opening in the small-Q limit. It will be shown that the simplified analysis in §3.2 provides a very good approximation to the upstream capture tube boundary despite the fact that the detailed velocity field over the hole is poorly described. Finally, we shall examine in §3.4 the limits of applicability of the various approximations by means of some numerical results.

3.1. *The case of strong suction*

It is not difficult to see that the cross-sectional dimensions of the capture tube along any (y, z)-plane, sufficiently far upstream of the pore are monotonically increasing functions of Q and that as $Q \to \infty$ these dimensions become infinite relative to the radius of the side branch. This also follows from the fact that, far from the pore, the flow field is that due to the linear superposition of a simple shear flow plus a flow due to a point sink at the origin of strength $2\pi Q$. Indeed, as $R \to \infty$, the velocity components as given by (1) and (2) reduce to

$$V_x = z - \frac{3Qxz^2}{(R^2+z^2)^{\frac{5}{2}}}, \quad V_y = -\frac{3Qyz^2}{(R^2+z^2)^{\frac{5}{2}}}, \quad V_z = -\frac{3Qz^3}{(R^2+z^2)^{\frac{5}{2}}}, \tag{4}$$

which indeed depicts the flow mentioned above.

It is evident from (4) that the strength of the shear flow becomes comparable with that of the sink flow if both z and R are of comparable magnitude $O(Q^{\frac{1}{3}})$. This, in turn, leads to the transformation

$$\tilde{z} = \frac{z}{(3Q)^{\frac{1}{3}}}, \quad \tilde{x} = \frac{x}{(3Q)^{\frac{1}{3}}}, \quad \tilde{y} = \frac{y}{(3Q)^{\frac{1}{3}}}, \quad \tilde{R} = \frac{R}{(3Q)^{\frac{1}{3}}}, \tag{5}$$

which reduces the equation for the streamlines to

$$\frac{\mathrm{d}\tilde{x}}{\mathrm{d}\tilde{z}} = \frac{\tilde{x}}{\tilde{z}} - \tilde{z}^3\left\{1+\frac{\tilde{R}^2}{\tilde{z}^2}\right\}^{\frac{5}{2}}, \quad \frac{\mathrm{d}\tilde{y}}{\mathrm{d}\tilde{z}} = \frac{\tilde{y}}{\tilde{z}}. \tag{6}$$

Hence, along a streamline, $\tilde{y} = \alpha\tilde{z}$ with α being an arbitrary constant parameter, and therefore, with $\eta \equiv -\tilde{x}/\tilde{z}$, we have that, in lieu of (6),

$$\frac{\mathrm{d}\eta}{\mathrm{d}\tilde{z}} = \tilde{z}^2\{1+\alpha^2+\eta^2\}^{\frac{5}{2}}. \tag{7}$$

This then is the equation for the streamlines in the 'outer' region whose linear dimensions are $O(Q^{\frac{1}{3}})$. The solution of (7) has to match of course with that of the inner

solution which applies within an $O(1)$ distance from the mouth of the pore where the flow is dominated by the suction velocity profile as $Q \to \infty$; but as we shall see presently, knowledge of this inner solution is not required to leading order in our analysis for the purpose of obtaining the capture tube cross-section at upstream infinity. In fact, the only pertinent information provided by this inner solution, which is required in the integration of (7), is that the slopes of all the streamlines entering the pore range from plus to minus infinity, and indeed, as we shall show presently, the solution to (7) yields an excellent approximation for the capture tube streamlines everywhere, except in the immediate vicinity of the pore mouth, when $Q > 1$.

Before deriving the general solution of (7), let us first consider the special case $\alpha = 0$, i.e. the streamlines lying within the $y = 0$ plane. Then, for all the streamlines which end at $\tilde{z} = \tilde{x} = 0$, we have, on integrating (7) with $\alpha = 0$, that

$$\tfrac{1}{3}\tilde{z}^3 = \int_{\eta_0}^{\eta} \frac{\mathrm{d}\eta}{(1+\eta^2)^{\frac{5}{2}}}, \tag{8}$$

where $-1/\eta_0$ equals the slope $\mathrm{d}\tilde{z}/\mathrm{d}\tilde{x}$ of a given streamline as z and x both approach zero. But, in view of what was said earlier about the flow in the inner region, $-\infty \leqslant \eta_0 \leqslant \infty$. In particular, $\eta_0 \to \pm\infty$ correspond to the streamlines approaching the origin along the negative and the positive x-axis, respectively. On evaluating the integral in (8) in closed form we then obtain that, for the dividing streamline in the $y = 0$ plane,

$$z^3 = 9Q \int_{-\infty}^{-x/z} \frac{\mathrm{d}\eta}{(1+\eta^2)^{\frac{5}{2}}} = 3Q\left[2 - \frac{3x}{(x^2+z^2)^{\frac{1}{2}}} + \frac{x^3}{(x^2+z^2)^{\frac{3}{2}}}\right]. \tag{9}$$

Consequently, as $x \to -\infty$, the far upstream height of the capture tube dividing streamline in the plane $y = 0$ is $Z_{-\infty} = (12Q)^{\frac{1}{3}}$. In an analogous fashion, we can easily show that, when $\alpha \neq 0$, the dividing stream surface is described by

$$z^3 = \frac{3Q}{(1+\alpha^2)^2}\left[2 - \frac{3x}{(x^2+y^2+z^2)^{\frac{1}{2}}} + \frac{x^3}{(x^2+y^2+z^2)^{\frac{3}{2}}}\right], \tag{10}$$

and that, as $x \to -\infty$, reduces to

$$Z_{-\infty}^3 = 9Q \int_{-\infty}^{\infty} \frac{\mathrm{d}\eta}{(1+\alpha^2+\eta^2)^{\frac{5}{2}}} = \frac{12Q}{(1+\alpha^2)^2} = 12Q\sin^4\theta, \tag{11}$$

where

$$\theta \equiv \tan^{-1}\left(\frac{Z_{-\infty}}{y}\right).$$

It should be noted that (11), describing the shape of the capture tube cross-section at upstream infinity, is independent of the size and the geometry of the pore, and thus is of general utility.

The dividing streamlines in the $y = 0$ plane given by (9) (solid lines) are compared in figure 4(*a*) with our numerical results using the method described in §2 (symbols). It is seen that the agreement is excellent almost everywhere for $Q \geqslant 10$ and that even for smaller values of Q, e.g. $Q = 1$, the deviation occurs only in the immediate vicinity of the pore entrance. In figure 4(*b*) the cross-sectional shapes of the capture tube obtained using (10) (solid lines) are compared with the numerical solution in §2

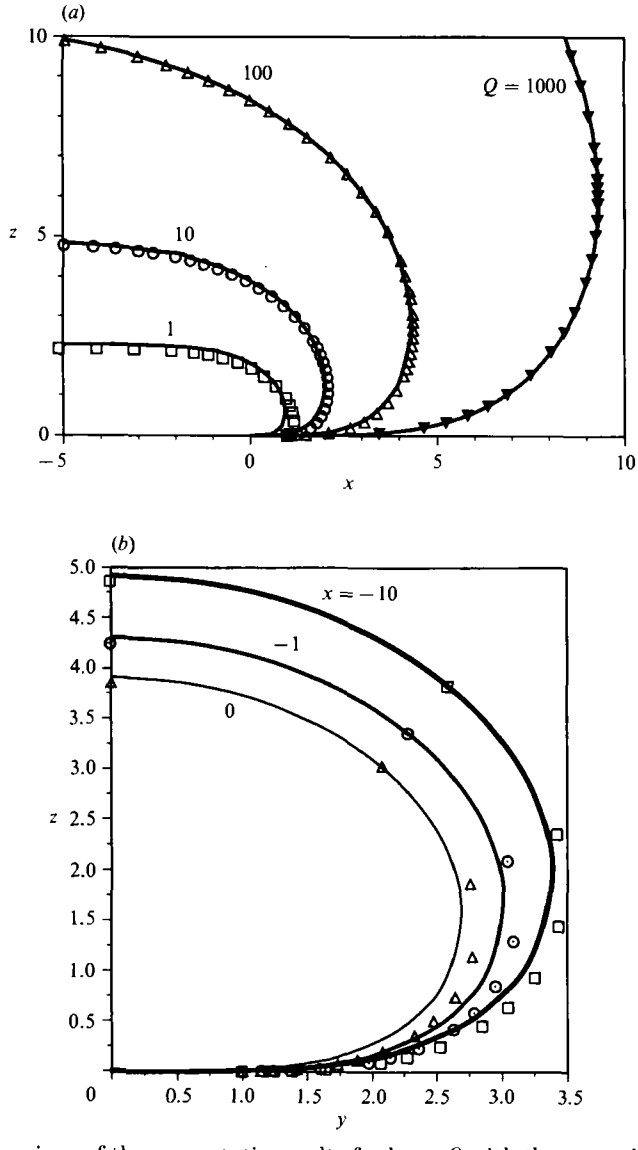

FIGURE 4. Comparison of the asymptotic results for large Q with the numerical ones. (*a*) Dividing streamlines in the $y = 0$ plane (symbols, numerical solution of (1), (2) and (3); solid lines, asymptotic). (*b*) Fluid capture tube cross-sections for $Q = 10$ (symbols, numerical solution of (1), (2) and (3); solid lines, asymptotic).

(symbols) for $Q = 10$ at different locations x. Clearly, except near the wall ($z = 0$), the two solutions are close to each other even for positions just over ($x = 0$) and just upstream ($x = -1$) of the pore mouth. This agreement suggests that for $Q > 1$ the very simple analytical formulae (9) and (11) will provide a surprisingly accurate approximation for the capture tube shape at all upstream locations.

We also note that the neglected terms in this asymptotic analysis are at least $O(Q^{-\frac{1}{3}})$ smaller than those which were retained and hence the relative error will vanish as $Q \to \infty$.

3.2. *The case of weak suction*

It is important to point out that the simplified velocity profile given by (1) and (2) cannot really be justified in the low-Q limit since the disturbance to the simple shear flow created by the presence of the hole dominates when $z \to 0$ and $0 \leqslant R \leqslant 1$. Nevertheless, we shall retain this simplified velocity profile in this subsection because the solution of the simplified set of equations for the streamlines will provide us with useful insight into how the correct asymptotic analysis should be performed in the next subsection for the exact flow pattern. In addition it will be seen that the predicted shapes of the capture tube cross-sections using this simplified profile will be almost identical to those obtained from the much more elaborate analysis using the full solution for the simple shear flow past an orifice or pore.

Now, returning to (1) and (2), we note that, when Q is small compared with unity, the flow field associated with the Sampson solution is negligible in strength relative to that of the shear flow unless $z \to 0$ and R is $O(1)$, i.e. near the entrance of the pore where both flows, although weak, are of comparable magnitude. Thus, the streamlines remain horizontal and parallel, to the first approximation, except near the entrance of the pore.

To obtain the dimensions of this 'inner' region, we observe from (1) and (2) that $V_x = z\{1 + O(Q)\}$ while V_y and V_z are both $O(Q)$. Hence, in view of (3), the equation for the streamlines within the 'inner' region is

$$\frac{\mathrm{d}z}{\mathrm{d}x} = O\left(\frac{Q}{z}\right), \quad \frac{\mathrm{d}y}{\mathrm{d}x} = O(Q) \quad \text{since} \quad V_y \to O(Qz) \quad \text{as} \quad z \to 0.$$

Hence the appropriate scaling in the inner region is

$$\bar{z} = zQ^{-\frac{1}{2}}, \quad \bar{R} = R, \tag{12}$$

in terms of which the equation for the streamlines reduces to

$$\frac{\mathrm{d}\bar{z}}{\mathrm{d}x} = \frac{\bar{V}_z(0)}{\bar{z}} + O(Q^{\frac{1}{2}}), \quad \frac{\mathrm{d}y}{\mathrm{d}x} = O(Q), \tag{13}$$

where

$$\bar{V}_z(0) = -\frac{3}{4}\frac{\zeta}{R}(R_1 - R_2)\left(\frac{R-1}{R_1} - \frac{R+1}{R_2}\right) = \begin{cases} -3(1-R^2)^{\frac{1}{2}} & \text{for} \quad 0 \leqslant R \leqslant 1 \\ 0 & \text{for} \quad R \geqslant 1 \end{cases}. \tag{14}$$

Thus, on integrating (13), we have that y remains constant along a streamline which enters the pore, while

$$\tfrac{1}{2}\bar{z}^2 = 3\int_x^{(1-y^2)^{\frac{1}{2}}} (1-x^2-y^2)^{\frac{1}{2}}\,\mathrm{d}x \quad \text{for} \quad -(1-y^2)^{\frac{1}{2}} \leqslant x \leqslant (1-y^2)^{\frac{1}{2}},$$

since $\bar{z} = 0$ when $x = (1-y^2)^{\frac{1}{2}}$, $-1 \leqslant y \leqslant 1$. Also $\mathrm{d}\bar{z}/\mathrm{d}x = 0$ when $x \leqslant -(1-y^2)^{\frac{1}{2}}$. Consequently, when $x \leqslant -(1-y^2)^{\frac{1}{2}}$ and therefore at upstream infinity, the cross-section of the capture tube is given to leading order (i.e. with an error of $O(Q^{\frac{1}{2}})$) by its shape at the upstream edge of the pore:

$$Z^2 \equiv Z^2_{-\infty} = 12Q\int_0^{(1-y^2)^{\frac{1}{2}}} (1-x^2-y^2)^{\frac{1}{2}}\,\mathrm{d}x = 3\pi Q(1-y^2) \quad \text{for} \quad x \leqslant -(1-y^2)^{\frac{1}{2}}. \tag{15}$$

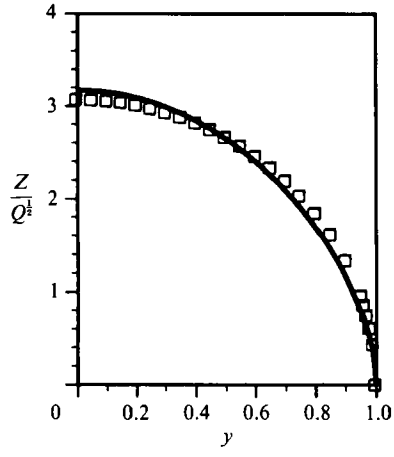

FIGURE 5. Comparison of the far upstream cross-section shapes using different velocity profiles at the pore mouth for small Q (solid line, using (15); symbols, using (17)).

It should be noted that, in contrast to the case of strong blowing where the shape of the capture tube cross-section is independent of the shape and dimensions of the pore, here the functional relation between $Z_{-\infty}$ and y is dependent on the size as well as the geometry of the pore, since the latter affects the suction velocity profile at $z = 0$ which in turn enters into (13), i.e. the equation for the streamlines within the inner region.

This analysis pertains of course to the case of flow into a circular orifice of zero thickness where the Sampson solution accurately represents the axial velocity at the pore entrance. On the other hand, when the pore has a length greater than about half its radius, then, as mentioned earlier, Dagan *et al.* (1982) have shown that the axial velocity at $z = 0$ is given to high accuracy by the arithmetic mean of the Sampson and Poiseuille profiles. Consequently, (14) should be replaced by

$$\bar{V}_z(0) \equiv \frac{V_z(0)}{Q} = -\tfrac{1}{2}[3(1-R^2)^{\frac{1}{2}} + 4(1-R^2)] \quad \text{for} \quad 0 \leqslant R \leqslant 1, \tag{16}$$

and, in place of (15), one obtains for the capture tube cross-section

$$Z^2 \equiv Z_{-\infty}^2 = Q[\tfrac{3}{2}\pi(1-y^2) + \tfrac{16}{3}(1-y^2)^{\frac{3}{2}}] \quad \text{for} \quad x \leqslant -(1-y^2)^{\frac{1}{2}}. \tag{17}$$

The cross-section shapes upstream of the pore mouth, as given by (15) and (17), are compared in figure 5 and are seen to be practically identical. This indicates that, even when $Q \ll 1$, the upstream capture tube shape is relatively insensitive to the velocity profile at the pore mouth.

3.3. *The influence of the disturbance flow past the hole*

The results just derived, and specifically (15) and (17), need to be more carefully analysed, however, since, as mentioned in the previous subsection, the use of (1) and (2) is of questionable validity in the low-Q limit because a simple shear flow past a hole will create a disturbance velocity along the x-direction which will remain $O(1)$ as $z \to 0$ and therefore should enter into the equation for the capture tube surface. To examine the effect of this disturbance, we shall utilize the exact velocity profile for the simple shear flow past a circular hole in a plane wall, recently derived by Davis (1991) and summarized in the Appendix.

We note that, as $z \to 0$, $0 \leqslant R \leqslant 1$, and in the absence of any suction,

$$V_z = \frac{2zx}{3\pi}(1-R^2)^{-\frac{1}{2}}, \quad V_x = \frac{2}{3\pi}(1-R^2)^{\frac{1}{2}}, \quad V_y = O(z), \tag{18}$$

and, therefore we obtain, in lieu of (13) that, as $Q \to 0$,

$$\frac{\mathrm{d}z}{\mathrm{d}x} = \frac{xz}{1-R^2} - \frac{9\pi Q}{2}, \quad \frac{\mathrm{d}y}{\mathrm{d}x} = O(Q), \tag{19}$$

where also included is the suction component $\bar{V}_z(0)$ as given by (14). The streamline which intersects the downstream edge of the orifice at $z = 0$ and $x = +(1-y_0^2)^{\frac{1}{2}}$, for $0 \leqslant y_0 \leqslant 1$, is then given by

$$z = \frac{9\pi}{2}\frac{Q}{(1-R^2)^{\frac{1}{2}}}\int_x^{(1-y_0^2)^{\frac{1}{2}}} (1-t^2-y^2)^{\frac{1}{2}}\,\mathrm{d}t \xrightarrow[x \to -(1-y_0^2)^{\frac{1}{2}}]{} \frac{9\pi^2}{4} Q \frac{1-y_0^2}{(1-R^2)^{\frac{1}{2}}}, \tag{20}$$

with $y = y_0$.

We see from (20) that z is now $O(Q)$ for $0 \leqslant R < 1$ rather than $O(Q^{\frac{1}{2}})$ as obtained in (15) or (17). In addition, when $x \to -(1-y_0^2)^{\frac{1}{2}}$, V_x and V_z, as given by (18), become comparable in magnitude when $r = |1-R|$ is $O(z)$ and therefore, in view of (20), both z and r become $O(Q^{\frac{2}{3}})$. In fact, within an $O(Q^{\frac{2}{3}})$ distance from the rim $R = 1$, all three velocity components are of $O(r^{\frac{1}{2}})$, and hence $O(Q^{\frac{1}{3}})$, and therefore large compared to the suction velocity which is of $O(Q)$. Also, one can show that in this region $\partial V_\varphi/\partial\varphi$ is of $O(r^{\frac{1}{2}})$, and therefore $O(Q^{\frac{2}{3}})$ smaller than either $\partial V_z/\partial z$ or $\partial V_R/\partial R$. Thus the flow within an $O(Q^{\frac{2}{3}})$ distance from the rim is effectively two-dimensional in the (z,R)-plane. Moreover, in this region the velocity components V_z and V_R must conform to the local solution of the Stokes equations for the two-dimensional symmetric flow past the trailing edge of a flat plate, whose stream function Ψ for $z \geqslant 0$ is given by Weinbaum (1968):

$$\Psi = -\frac{\sqrt{2}}{3\pi}\rho^{\frac{3}{2}}\{\sin\tfrac{1}{2}\theta + \sin\tfrac{3}{2}\theta\}\cos\varphi, \quad \text{with } \theta \equiv \tan^{-1}\left(\frac{z}{r}\right), \quad \rho \equiv (r^2+z^2)^{\frac{1}{2}}, \tag{21a}$$

where the proportionality constant was determined by requiring that, in view of (18),

$$\Psi \to -\frac{2\sqrt{2}}{3\pi} r^{\frac{3}{2}}\theta\cos\varphi \quad \text{as} \quad \theta \to 0. \tag{21b}$$

Using (20) and (21*b*), we also find that, as $(1-R^2)^{\frac{1}{2}} \to 0$, the capture tube surface streamlines are given by

$$\Psi = -\tfrac{3}{2}\pi Q(1-y_0^2)\cos\varphi.$$

But, as $\theta \to \pi$, we have from (21*a*) that

$$\Psi \to -\frac{\sqrt{2}}{3\pi} r^{\frac{3}{2}}(\pi-\theta)^2\cos\varphi = -\frac{\sqrt{2}}{3\pi}\frac{z^2}{(R-1)^{\frac{1}{2}}}\cos\varphi \quad \text{for} \quad R > 1,$$

and since, from continuity, these last two expressions must be equal to each other, we have, along the surface of the capture tube,

$$z = \tfrac{3}{2}\pi(R^2-1)^{\frac{1}{4}}Q^{\frac{1}{2}}(1-y_0^2)^{\frac{1}{2}} \quad \text{as} \quad R \to 1. \tag{22}$$

Also, y has remained equal to y_0.

Finally, as R is increased beyond the rim, the undisturbed linear shear flow velocity, which up to now had played no role in the present analysis, attains increasing importance. Integrating the streamline equations using the velocity components (A 3), one can show that, for $R > 1$,

$$\frac{y}{y_0} = \exp\left(\int_1^{R^2} \frac{\mathrm{d}t}{A(t)}\right), \quad z = \tfrac{3}{2}\pi Q^{\frac{1}{2}}(1-y_0^2)^{\frac{1}{2}}\left(1-\frac{1}{R^2}\right)^{\frac{1}{4}} \exp\left[\int_1^{R^2} \frac{t}{t-1}\left(\frac{1}{A(t)}-\frac{1}{4t^2}\right)\mathrm{d}t\right], \tag{23a}$$

with

$$A(t) \equiv 3\pi t^2(t-1)^{\frac{1}{2}} - 3t^2(t-1)^{\frac{1}{2}}\sin^{-1}\left(\frac{1}{t^{\frac{1}{2}}}\right) + 3t^2 + t, \tag{23b}$$

where we have imposed the conditions that, as $R \to 1$, the above expression for z reduces to (22) and that $y = y_0$. Numerical evaluation of the first integral in (23a) gives that, as $R \to \infty$, $y \to \sigma y_0$ where $\sigma = 1.10$. In addition, since $V_x \to z$ as $R \to \infty$, the integral of z over the capture tube cross-section far upstream must be equal to $2\pi Q$. Thus, one obtains from (23b)

$$Z_{-\infty}^2 = \frac{3\pi}{\sigma} Q\left(1-\frac{y^2}{\sigma^2}\right) \quad \text{with} \quad \sigma = 1.10, \tag{24}$$

which is identical to (15) except for the shape factor $\sigma = 1.10$. Therefore, the capture tube cross-section is again an ellipse, but with a slightly different eccentricity. We can conclude, therefore, that the details of the flow over the hole have surprisingly little effect on the upstream capture tube boundary even in the low-Q limit, and that the simplified velocity field used in (1) and (2) provides an approximation which is more than adequate.

We next consider the flow past a side pore of finite length. In the absence of suction, the disturbance flow velocity has the same dependence on the angle φ as in the case of flow past an orifice in that V_z and V_R are proportional to $\cos\varphi$ while V_φ is proportional to $\sin\varphi$. In addition, we find from Tutty's numerical solution that, at $z = 0$, the x-component of the disturbance velocity can be accurately represented by means of

$$V_x(x, y, 0) \approx 0.16(1-R^2)^{0.544} \quad \text{for} \quad 0 \leqslant R \leqslant 1, \tag{25}$$

where we have chosen the exponent to equal 0.544 in order to ensure that, as $R \to 1$, the form of $V_x(x, y, 0)$ be compatible with that of the known local solution of the Stokes equations for flow past a 90° blunt-based trailing edge (Weinbaum 1968). In addition, the fact that $V_x(x, y, 0)$ is essentially a function of R alone implies that $V_y(x, y, 0)$ vanishes. On the other hand, $V_z(x, y, 0)$ is now finite and is an odd function of x. Hence, in the low-Q limit, we obtain, in lieu of (19), that

$$\frac{\mathrm{d}z}{\mathrm{d}x} = \frac{V_z(x, y, 0)}{0.16(1-R^2)^{0.544}} - \frac{1.088zx}{1-R^2} + \frac{Q\bar{V}_z(0)}{0.16(1-R^2)^{0.544}}, \tag{26}$$

where $Q\bar{V}_z(0)$ is the suction flow profile at the pore entrance given by (16) and the first two terms on the right-hand side are obtained from a Taylor series expansion of $V_z(x, y, z)$ about the plane $z = 0$ and from application of the continuity equation.

It might appear at this stage that the integration of (26) would encounter serious difficulties because, in the neighbourhood of the pore entrance, $\mathrm{d}y/\mathrm{d}x = V_y/V_x = O(z)$ along a streamline and thus does not vanish as $Q \to 0$. Therefore, for $0 \leqslant R \leqslant 1$, a given streamline is no longer confined to lie within an (x, z)-plane as was the case for

the orifice, and y no longer remains equal to y_0. Fortunately, we see from Tutty's (1988) numerical solution that, although $V_z(x, y, 0)$ is finite, it is an order of magnitude smaller than $V_x(x, y, 0)$ everywhere except near the rim $R = 1$ where both vanish at the same rate. Thus, even though the separation streamlines do not detach at the trailing edge when $Q = 0$ (Weinbaum 1968; Tutty 1988), they remain everywhere close to the surface $z = 0$ and therefore, $\mathrm{d}y/\mathrm{d}x$, although not zero, will be small along any one of them. In turn, this implies that letting $y = y_0$ in (26) should constitute an acceptable approximation.

Before proceeding, let us examine the local solution near the rim with which the solution of (26) has to match. We have (Weinbaum 1968) that, by analogy with (21*a*),

$$\Psi = -B\rho^m\{\cos m(\theta-\tfrac{1}{4}\pi)+\cot(\tfrac{3}{4}m\pi)\cos[(m-2)(\theta-\tfrac{1}{4}\pi)]\}\cos\varphi+O(\rho^n), \qquad (27)$$

with $m = 1.544$, where the neglected term with $n = 1.91$ describes the lowest-order antisymmetric component of the no-suction solution. Although this term is required to determine the separation streamlines beneath the trailing edge, the $O(\rho^m)$ term in (27) dominates the flow along the plane $z = 0$ as $\rho \to 0$ and hence the influence of the *antisymmetric* solution can be neglected for the purpose of this analysis.

The coefficient B in (27) can be found by requiring that $\partial\Psi/\rho\,\partial\theta$ become equal to $-0.16\times 2^{m-1}\rho^{m-1}\cos\varphi$ as $\theta \to 0$. Therefore, on noting that, since $V_z(x, y, 0)$ is odd in x and in view of (27),

$$\int_x^{(1-y_0^2)^{\frac{1}{2}}} \frac{V_z(x, y_0, 0)\,\mathrm{d}x}{0.16(1-x^2-y_0^2)^{m-1}} \to Cr \quad \text{as} \quad x \to -(1-y_0^2)^{\frac{1}{2}} \quad \text{and} \quad r = 1-R,$$

where C is an $O(1)$ numerical constant which need not be determined. We then obtain on integrating (26) that, as $x \to -(1-y_0^2)^{\frac{1}{2}}$ and with $m-1 = 0.544$,

$$z \to \frac{Cr}{(1-R^2)^{m-1}} + \frac{Q[\frac{3}{4}(1-y_0^2)+\frac{8}{3}(1-y_0^2)^{\frac{3}{2}}]}{0.16(1-R^2)^{m-1}}.$$

Finally, by repeating the steps of the earlier analysis in connection with the problem of flow past an orifice, we can easily show that the cross-section of the capture tube at upstream infinity is given by

$$Z_{-\infty}^2 = \frac{Q}{\xi}\left[\frac{3}{2}\pi\left(1-\frac{y^2}{\xi^2}\right)+\frac{16}{3}\left(1-\frac{y^2}{\xi^2}\right)^{\frac{3}{2}}\right], \qquad (28)$$

where the value of ξ can be obtained, as was done earlier with the quantity σ, through knowledge of the disturbance to the simple shear flow created by the hole. Although, the solution for this disturbance is not known, it appears safe to assume that ξ cannot differ all that much from 1.10, as indicated in fact by Tutty's numerical solution for $Q = 0.005$ shown in figure 3. Thus (17) and (28) are practically the same.

We can see then that, once again, the use of a more exact expression for the velocity profile has led to a change in the shape of the capture tube cross-section at upstream infinity which is negligible for practical purposes. Hence, in what follows, we shall proceed with our analysis on the basis of the simplified form for the velocity as given by (1) and (2) even when Q is small.

3.4. *Discussion of the asymptotic expressions*

In the previous subsection we have derived asymptotic expressions for the shape of the upstream capture tube cross-section when Q becomes either very large or very small. Specifically, we have shown that (11) applies when $Q \to \infty$ irrespective of the

	$Z_{-\infty}$ values in the $y = 0$ plane			
Q	Numerical sol.	Eq. (11)	Eq. (15)	Eq. (30)
50	8.40	8.43		8.41
10	4.87	4.93		4.49
5	3.84	3.91		3.86
1	2.17	2.29		2.18
0.5	1.68	1.82		1.68
0.17	1.10	1.27	1.27	1.10
0.100	0.873		0.971	0.872
0.050	0.643		0.687	0.641
0.010	0.302		0.307	0.300
0.005	0.215		0.217	0.214
0.001	0.0969		0.0971	0.0967

TABLE 1. Comparison between numerical and asymptotic results for the capture tube heights in the $y = 0$ plane at upstream infinity

geometry or the dimensions of the hole, while as $Q \to 0$, we have (15) or (24) for the orifice and (17) or (28) for the pore with very little difference amongst them. However, since the intersection of (15) and (11) in the plane $y = 0$ occurs at

$$Q = \frac{16}{3\pi^3} \approx 0.17, \quad Z_{-\infty} \approx 1.27, \tag{29}$$

we can estimate the shape of the far upstream capture tube by means of (15) or (17) (with little difference between the two) when $0 < Q < 0.17$, and by means of (11) when $Q \geqslant 0.17$. The results in the previous subsection for $Q \ll 1$ can also be used to explain why our far upstream capture tube shape for $Q = 0.005$ in figure 3 agreed so well with that computed by Tutty even though, at this low suction rate, this flow field at the pore mouth differs drastically from that employed in our simplified analysis, which led to (15).

The results of our numerical solution discussed in §2 are compared in table 1 with the predictions given by two of the asymptotic expressions, (11) and (15). It can be seen that, over the appropriate range of Q as defined by (29), the respective asymptotic expressions are in close agreement with the numerical values for the far upstream capture tube height $Z_{-\infty}$ in the $y = 0$ plane with a relative error of less than 2% when $Q < 0.025$ or $Q > 2.5$. In fact, as is evident from this table, the asymptotic solutions (11) and (15) always overpredict the capture tube height at $y = 0$. Thus it is possible to represent the numerical results by means of the simple interpolation formula

$$Z_{-\infty} = (Z_1^n + Z_2^n)^{1/n}, \quad n = -4.67, \tag{30}$$

where $Z_1 = (12Q)^{\frac{1}{3}}$ and $Z_2 = (3\pi Q)^{\frac{1}{2}}$ are the two asymptotic expressions for $Z_{-\infty}$ in the $y = 0$ plane, given by (11) and (15), respectively. As is also shown in table 1, the values for $Z_{-\infty}$ computed by means of (30) are in exceptionally close agreement with those of our numerical solution for all values of Q with a maximum relative error of only 0.4%.

It is important to point out that although the numerical values of $Z_{-\infty}$ in the $y = 0$ plane fall everywhere slightly below those given by the appropriate asymptotic expressions even in the intermediate range when Q is neither very large nor very small, the cross-sectional shape of the capture tube changes markedly from one limit

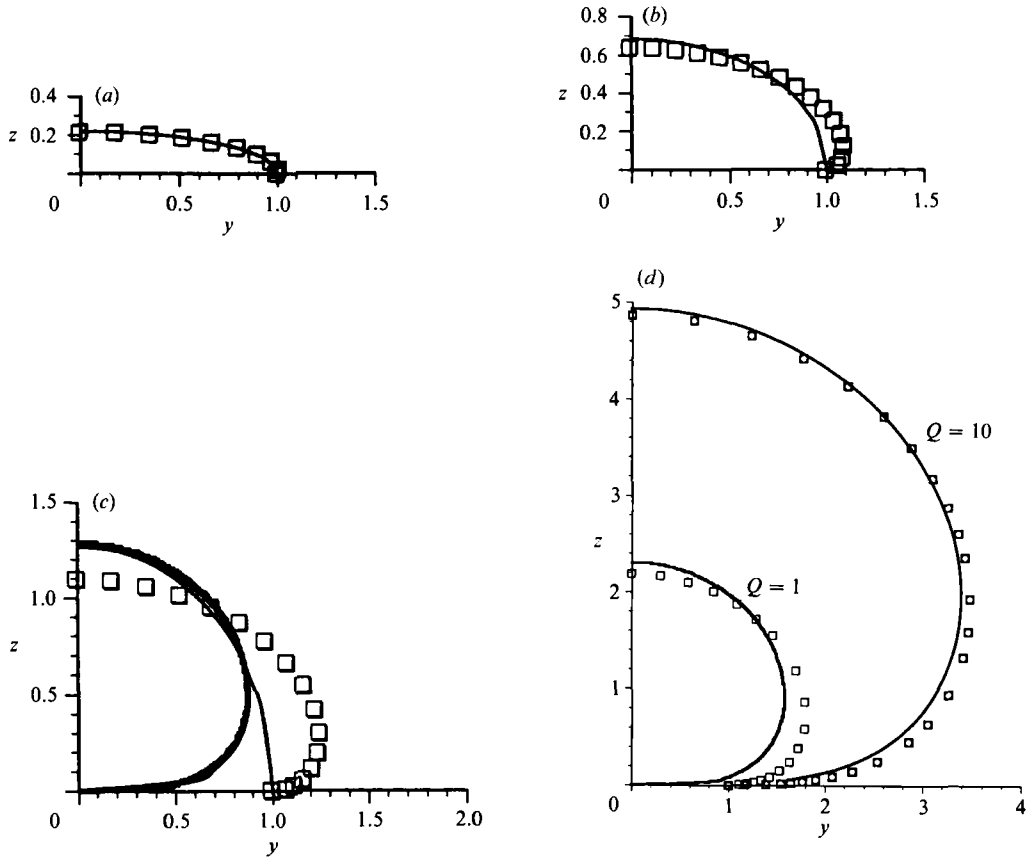

FIGURE 6. The variation of the cross-section shape of the fluid capture tube with Q and comparison with the asymptotic results (symbols, numerical solution of (1), (2) and (3); thin line, using (15); bold line, using (11)). (*a*) $Q = 0.005$; (*b*) $Q = 0.05$; (*c*) $Q = 0.172$; (*d*) $Q = 1$ and $Q = 10$.

to the other. Interpolating between the curves in figure 6, one observes that, when $Q < 0.1$ this cross-sectional shape is accurately represented by the weak suction asymptotic solution, (15), i.e. it is an ellipse which becomes more and more oblate as Q decreases while, when $Q > 2$, the shape corresponds to that given by the large suction asymptotic solution, (11). In the intermediate range of Q, however, the cross-sectional shape is not well represented by either asymptotic formula. This suggests that although the asymptotic solutions can accurately predict the capture tube height in the $y = 0$ plane even in the intermediate range of Q, the numerical solution in §2 is still required to adequately describe other phenomena related to the capture tube shape in this range of Q, such as the plasma skimming effect which will be discussed in the next section.

4. Fluid skimming effect

Now let us consider a suspension of spherical particles of radius a and of uniform concentration $C_{-\infty}$ flowing under shear past a wall with small pores. The suspension is assumed to be so dilute that the flow field, the streamlines and the fluid capture tube will remain practically the same as described in §§2 and 3 for a pure fluid. However, for the case of a suspension, there exists a particle-free layer near the wall

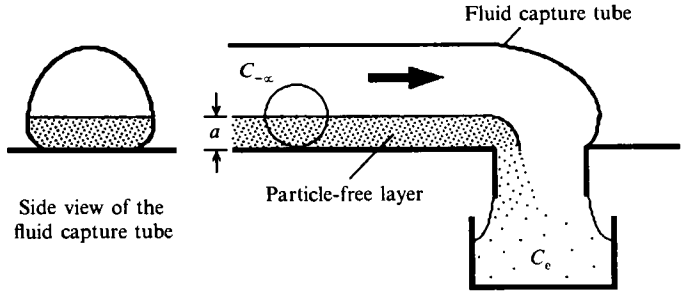

FIGURE 7. Diagram showing the plasma skimming effect.

for $z \leqslant a$ and $x \leqslant -(1-y^2)^{\frac{1}{2}}$, as indicated by the shaded region in figure 7. Then within the capture tube, whose total flux through the pore is $2\pi Q$, the part from the shaded region, whose flux is denoted by $2\pi Q_a$, does not carry particles. Hence, if the particle size a is comparable with the capture tube height, the average particle concentration at the pore exit, C_e, will be lower relative to the far upstream value $C_{-\infty}$ even if the hydrodynamic interaction between the particles and the boundary is neglected. This hydrodynamic interaction will be considered in Wu *et al.* (1991); but, for the pure fluid skimming effect treated in this section, the particles will be assumed to move with the average velocity of the undisturbed fluid which is displaced by their volume. In the microcirculation this fact is believed to be largely responsible for the well-known observation that blood which is discharged from a tiny branch vessel will contain a smaller population of cells and thus be richer in plasma. This is usually called the plasma skimming effect, but since our discussion is not limited to the microcirculation, this effect will be referred to in this paper as fluid skimming.

It is evident from figure 7 that mass conservation for the particle phase requires that

$$\frac{C_e}{C_{-\infty}} = \frac{Q-Q_a}{Q}. \tag{31}$$

For a general given value of Q, Q_a must be computed numerically based on the capture tube cross-section shape and the fluid velocity at a far upstream location as described in §2. However, for the large- and small-Q limits, closed-form results can be obtained from the asymptotic analytical solutions just presented in §3. Thus, for the case of small suction ($Q \ll 1$), using (15) for the capture tube shape (see figure 8*a*) and letting $V_x \approx z$ at far upstream locations, we have, for $a \leqslant (3\pi Q)^{\frac{1}{2}}$, that

$$2\pi(Q-Q_a) = \int_0^{y_a}\int_a^z z\,\mathrm{d}z\,\mathrm{d}y = 3\pi Q y_a - \pi Q y_a^3 - a^2 y_a,$$

where $y_a = [1-(a^2/3\pi Q)]^{\frac{1}{2}}$. On the other hand, if $a > (3\pi Q)^{\frac{1}{2}}$, then the whole capture tube falls within the particle-free layer and thus the discharge fluid from the pore will contain no particles at all. Hence we obtain for the small-Q limit and, after making use of the above expression for y_a, that

$$\frac{C_e}{C_{-\infty}} = \begin{cases} \left(1-\dfrac{a^2}{3\pi Q}\right)^{\frac{3}{2}} & \text{if} \quad Q > \dfrac{a^2}{3\pi}; \\ 0 & \text{if} \quad 0 \leqslant Q \leqslant \dfrac{a^2}{3\pi}. \end{cases} \tag{32}$$

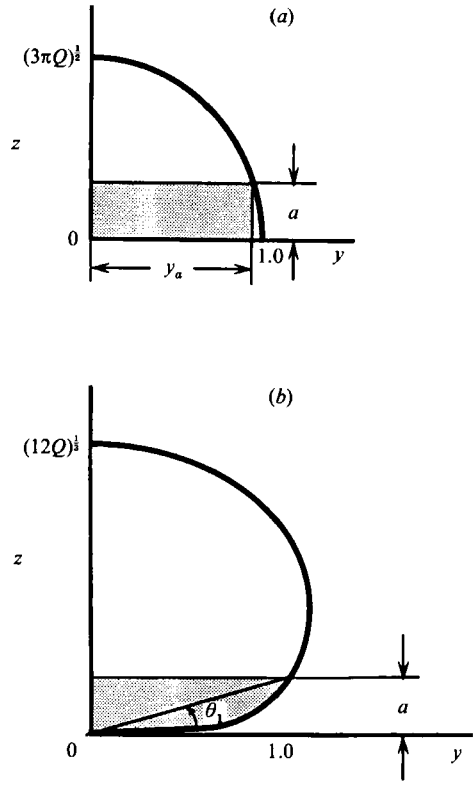

FIGURE 8. Diagram illustrating evaluation of the flux in fluid capture tube: (*a*) small suction case; (*b*) strong suction case.

At the other extreme, that of strong suction ($Q \gg 1$), we use (11) for the capture tube shape (see figure 8*b*) to obtain

$$2\pi(Q-Q_a) = 2\int_{\theta_1}^{\pi/2}\int_{a/\sin\theta}^{(12Q\sin\theta)^{\frac{1}{3}}} (r\sin\theta)\, r\,\mathrm{d}r\,\mathrm{d}\theta$$
$$= 2\pi Q - 4Q\theta_1 + 2Q\sin(2\theta_1) - \tfrac{2}{3}a^3\cot\theta_1,$$

where $\theta_1 = \sin^{-1}(a^3/12Q)^{\frac{1}{4}}$. When expanded into Taylor's series in powers of $(a^3/12Q)^{\frac{1}{4}}$ the above expression becomes in the large-Q limit

$$\frac{C_e}{C_\infty} = 1 - 0.2633\left(\frac{a^3}{Q}\right)^{\frac{3}{4}} + O(Q^{-\frac{13}{12}}), \tag{33}$$

where the third term on the right-hand side is as indicated because, as remarked in §3, the relative error in the asymptotic strong suction analysis, and therefore, in the expression for θ_1 given above is $O(Q^{-\frac{1}{3}})$.

Figure 9 depicts the variation of $C_e/C_{-\infty}$ with the side branch flux $2\pi Q$ and the particle radius a. It can be seen that our numerical results approach those of the asymptotic solution, (32) or (33), very rapidly as $Q \to 0$ or $Q \to \infty$, respectively. Furthermore, for any given value of Q and of a, these two asymptotic expressions when combined provide a reasonable estimate for $C_e/C_{-\infty}$. In fact, the values of $C_e/C_{-\infty}$ computed from the numerical solutions lie invariably below the asymptotic

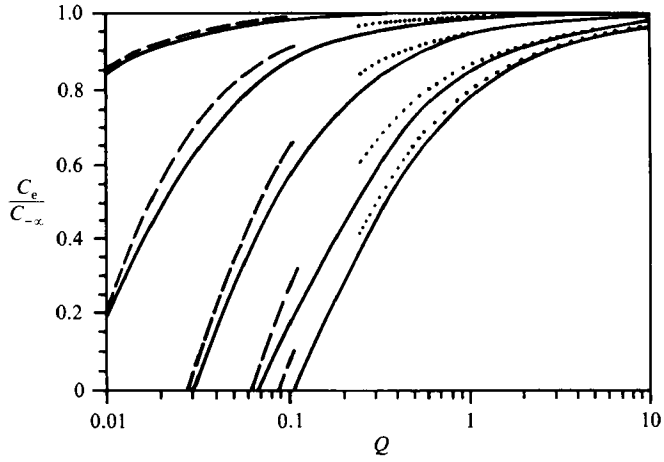

FIGURE 9. The fluid skimming effect (solid lines, numerical results using (31); dashed lines, using (32); dotted lines, using (33). Starting from the top are curves for $a = 0.10, 0.25, 0.50, 0.75$ and 0.90, respectively.

expressions which therefore serve as the upper limit. It is also seen that when the particle size a is fixed, $C_e/C_{-\infty}$ increases monotonically with increasing Q and that as Q increases indefinitely, $C_e/C_{-\infty}$ will asymptote to unity for all $a < 1$ (i.e. the particle-free layer will constitute then only a negligible portion of the capture tube). Moreover, in the low-Q limit, $C_e/C_{-\infty}$ will vanish as Q approaches $Q_{\min} = a^2/3\pi$, even though the particle diameter may be smaller than the pore opening (i.e. the whole capture tube will fall within the particle-free layer). This intriguing result suggests that for $Q \ll 1$ it should be possible to skim off the fluid phase without loss of suspended particles even when these are smaller than the size of the pores (e.g. for $a = 0.5$, the discharge will not contain particles when $Q < 0.0265$ if the hydrodynamic interaction between the particles and the wall is neglected). Finally, when Q is fixed, $C_e/C_{-\infty}$ decreases with increasing a because of the thickening of the particle-free layer.

5. Effect of non-zero pore length on the wall shear stress

The analysis presented thus far has dealt primarily with the flow past an orifice of zero length and thus a simplified velocity field consisting of a simple shear flow plus a Sampson's flow was utilized. But, as discussed in §3 as well as demonstrated numerically, the far upstream capture tube shape is altered only slightly if use is made of (16), i.e. the velocity profile at the mouth of a finite-length pore given by Dagan *et al.* (1982). Similarly, the use of the exact velocity for the shear flow past a pore in lieu of the undisturbed linear shear flow was found to have a very small effect. This means that the analysis in §4 for the fluid skimming effect remains essentially valid irrespective of the actual pore length. On the other hand, the presence of a non-zero pore length does influence the topology of the streamlines near the pore entrance and, in particular, the locus of the downstream attachment boundary for the capture tube. Recall that the numerical solutions in Tutty (1988) have shown that, when $Q \gg 1$, this attachment boundary is located at a significant distance downstream from the edge of the pore. This fact is of considerable interest in studies concerning atherogenesis (Tutty 1988; Cornhill & Roach 1976), where

attempts have been made to relate the local wall shear and the location of the attachment point to the pattern of early lesion formation. In this section we shall derive a closed-form asymptotic expression for evaluating the wall shear rate and use this expression to determine the location of the attachment boundary contours. This simple closed-form solution will turn out to be surprisingly accurate for almost all Q-values of practical interest.

By taking the Fourier transform in x and y and the Laplace transform in z of the Stokes equations, it is possible to show that the x-component of the fluid velocity in the upper half-space $z \geqslant 0$ may be expressed as (Sobey 1977; Tutty 1988)

$$V_x = z + \frac{3}{2\pi} \iint_{\substack{R' \leqslant 1 \\ z'=0}} \frac{(x-x')\, zK(x,y,z,x',y')}{[(x-x')^2+(y-y')^2+z^2]^{\frac{5}{2}}} \,\mathrm{d}x'\,\mathrm{d}y', \tag{34}$$

where $R' = (x'^2+y'^2)^{\frac{1}{2}}$ and

$$K(x,y,z,x',y') = (x-x')\, V_x(x',y',0) + (y-y')\, V_y(x',y',0) + zV_z(x',y',0).$$

Thus, once the velocity profiles at the pore mouth ($R' \leqslant 1$, $z' = 0$) are given, it is an easy matter to find the locus of the fluid streamline attachment boundary, defined by $\tau_{\text{wall}} = \mu(\partial V_x/\partial z)_{z=0} = 0$. In Tutty (1988) the velocity profiles at the pore mouth were taken from his numerical results and the double integration in (34) was performed numerically. But, as we shall show presently, this numerical integration can be replaced by a simple and accurate closed-form expression.

To this end, differentiating (34) we have that

$$\left(\frac{\partial V_x}{\partial z}\right)_{\substack{z=0 \\ R>1}} = 1 + \frac{3}{2\pi} \iint_{\substack{R' \leqslant 1 \\ z'=0}} \frac{(x-x')\,[(x-x')\, V_x(x',y',0) + (y-y')\, V_y(x',y',0)]}{[(x-x')^2+(y-y')^2]^{\frac{5}{2}}} \,\mathrm{d}x'\,\mathrm{d}y', \tag{35}$$

where the velocity profiles $V_x(x',y',0)$ and $V_y(x',y',0)$ consist of the superposition of an axisymmetric fluid suction into the pore and a shear flow past the pore without suction. For the axisymmetric suction, these profiles may be expressed in terms of a single radial velocity component at the pore mouth, $V_R^0(R')$, which is independent of φ':

$$V_x(x',y',0) = V_R^0(R')\cos\varphi', \quad V_y(x',y',0) = V_R^0(R')\sin\varphi'.$$

For the no-suction shear flow, $V_x(x',y',0)$ is a function of R' alone, which is accurately described by (25), and $V_y(x',y',0)$ may be taken to be zero for the reason indicated earlier. Numerical evaluation of (35) shows, however, that when $Q \geqslant 2$, the contribution to the wall shear stress due to the no-suction shear flow becomes negligible compared with that arising from the axisymmetric suction and, therefore, the shear flow component can be omitted without affecting the results significantly. Furthermore, since the location of the attachment boundary lies only slightly beyond the edge of the pore for $Q < 2$, it is reasonable to omit the contribution due to the no-suction shear flow for all problems in which the topology of the attachment boundary is of practical importance. Introducing this simplification, transforming the integrand of (35) into the cylindrical coordinate system (R', φ', z') and performing the integration over φ' analytically, one obtains

$$\left(\frac{\partial V_x}{\partial z}\right)_{\substack{z=0 \\ R>1}} = 1 - \frac{6Q}{\pi} J(R)\cos\varphi, \tag{36}$$

where

$$J(R) = \int_0^1 \left\{ (R^2+R'^2)\,[G_0(k)-2G_2(k)] - RR'[2G_0(k)-4G_2(k)+4G_4(k)]\,\frac{V_R^0(R')}{(R+R')^5}\,R'\,\mathrm{d}R' \right\}, \tag{37}$$

and $G_n(k)$ is defined as

$$G_n(k) \equiv \int_0^{\pi/2} \frac{\cos^n t\,\mathrm{d}t}{(1-k^2\sin^2 t)^{\frac{5}{2}}}, \quad k^2 = \frac{4RR'}{(R+R')^2}.$$

These functions $G_n(k)$ can be expressed in terms of the complete elliptic integrals of first and second kinds, $K(k)$ and $E(k)$, by means of

$$G_0(k) = \frac{2(k'^2+1)}{3k'^2}E(k) - \frac{1}{3k'^2}K(k),$$

$$G_2(k) = \frac{1}{3k^2}K(k) + \frac{2k^2-1}{3k^2k'^2}E(k),$$

$$G_4(k) = \frac{2+k^2}{3k^4}K(k) - \frac{2(1+k^2)}{3k^2k'^2}E(k),$$

where $k' = (1-k^2)^{\frac{1}{2}}$. When $k^2 \leqslant 10^{-4}$, the expressions given above become inaccurate owing to rounding-off errors and hence it is preferable to use the leading terms in a Taylor series expansion of the elliptic integrals for small k^2. This results in

$$G_0(k) = \tfrac{1}{2}\pi[1+\tfrac{5}{4}k^2+O(k^4)],$$
$$G_2(k) = \tfrac{1}{2}\pi[\tfrac{1}{2}+\tfrac{5}{16}k^2+O(k^4)],$$
$$G_4(k) = \tfrac{1}{2}\pi[\tfrac{3}{8}+\tfrac{5}{32}k^2+O(k^4)].$$

In the expression for $J(R)$, (37), the velocity profile $V_R^0(R')$ has yet to be specified. An accurate solution for $V_R^0(R')$ has been obtained in the form of an infinite series in Dagan *et al.* (1982) and is shown in their figure 6. But, a careful examination of the streamline pattern in figure 3 of Dagan *et al.* (1982) suggests that for a finite length pore, whose length is greater than half the pore radius ($L/c > 0.5$), the slope of the streamlines in the plane of the pore opening will be nearly the same as that for a Sampson's flow on a judiciously chosen oblate spheroidal coordinate surface which lies upstream of the entrance. In addition, numerical tests have shown that the shape of the radial velocity profile can be accurately fitted by means of Sampson's transverse velocity profile on the oblate coordinate surface $\lambda = 0.65$, where $\lambda = (\frac{1}{4}(R_1+R_2)^2-1)^{\frac{1}{2}}$ and R_1, R_2 are defined following (2), provided the maximum velocity is scaled so as to satisfy the magnitude of the peak radial velocity in Dagan *et al.*'s solution. It is found that the fitting formula

$$V_R^0(R') = 1.15Q\frac{R'(1-R'^2)}{1.42-R'^2} \tag{38}$$

provides a simple but highly accurate approximation for the radial velocity profile in figure 6 of Dagan *et al.* (1982).

When (38) for $V_R^0(R')$ is substituted into (37), the single integral (37) can be evaluated numerically and the attachment boundary contour $R = f(\varphi)$ located by imposing the condition $\tau_{\text{wall}} = \mu(\partial V_x/\partial z)_{z=0} = 0$. However, from (36), one expects that R should become large as $Q \to \infty$ provided $\cos\phi \neq 0$. Thus, for $Q \gg 1$, one can

φ (deg.)		$Q = 2$	$Q = 5$	$Q = 10$	$Q = 100$	$Q = 1000$
	$R = (\frac{1}{3}Q\cos\varphi)^{\frac{1}{4}}$	—	1.136	1.351	2.403	4.273
0	Eq. (41)	1.194	1.367	1.545	2.512	4.334
	Numerical	1.199	1.370	1.548	2.513	4.335
	$R = (\frac{1}{3}Q\cos\varphi)^{\frac{1}{4}}$	—	1.063	1.264	2.248	3.998
40	Eq. (41)	1.155	1.309	1.471	2.365	4.064
	Numerical	1.161	1.314	1.474	2.366	4.064
	$R = (\frac{1}{3}Q\cos\varphi)^{\frac{1}{4}}$	—	—	—	1.551	2.758
80	Eq. (41)	1.032	1.091	1.173	1.720	2.853
	Numerical	1.032	1.096	1.178	1.722	2.854
	$R = (\frac{1}{3}Q\cos\varphi)^{\frac{1}{4}}$	—	—	—	—	1.553
89	Eq. (41)	1.126	1.047	1.025	1.173	1.722
	Numerical	1.000	1.002	1.009	1.178	1.724

TABLE 2. The attachment boundary contours $R = f(\varphi)$

evaluate the integral (37) and thereby derive a closed-form expression for the asymptotic behaviour of $J(R)$ by expanding the functions $G_n(k)$ as Taylor series in k^2 followed by an expansion of k^2 in R'/R:

$$k^2 = \frac{4R'}{R}\left(1 - \frac{2R'}{R} + \frac{3R'^2}{R^2} + O\left(\frac{R'^3}{R^3}\right)\right).$$

It is found that

$$J(R) = \frac{0.1748}{R^4} + \frac{0.1831}{R^6} + O\left(\frac{1}{R^7}\right). \tag{39}$$

Substituting (39) into (36) and applying the condition $\tau_{\text{wall}} = \mu(\partial V_x/\partial z)_{z=0} = 0$, one finds that the attachment boundary contour is described by

$$R = \left\{\tfrac{1}{3}Q\cos\varphi\left[1 + \frac{1.047}{R^2} + O\left(\frac{1}{R^3}\right)\right]\right\}^{\frac{1}{4}}$$

$$= (\tfrac{1}{3}Q\cos\varphi)^{\frac{1}{4}}\left[1 + \frac{0.262}{R^2} + O\left(\frac{1}{R^3}\right)\right], \tag{40}$$

which can be solved by iteration to yield an explicit solution for R as a function of φ.

Thus, one obtains after one iteration that

$$R = (\tfrac{1}{3}Q\cos\varphi)^{\frac{1}{4}} + 0.262(\tfrac{1}{3}Q\cos\varphi)^{-\frac{1}{4}} + O(Q^{-\frac{1}{2}}). \tag{41}$$

Although the asymptotic expressions (41) is derived under the assumption that $Q \to \infty$ and $\cos\varphi \neq 0$ so that $R'/R \ll 1$, one finds that the solution to $\tau_{\text{wall}} = \mu(\partial V_x/\partial z)_{z=0} = 0$ using (41) is in surprisingly good agreement with the equivalent solution obtained from an exact numerical evaluation of $J(R)$ for values of Q as small as $Q = 2$ in the range of $|\varphi| \leqslant 80°$ (see table 2). In fact, for $Q \geqslant 10^3$ the first term in (41) deviates from the exact numerical solution by less than 3% *for* $|\varphi| \leqslant 80°$ and about 10% for $|\varphi| = 89°$. Considering that the attachment boundary contours converge to $R = 1$ as $|\varphi| \to 90°$ for all values of Q, the above agreement suggests that the very simple analytical expression, (41), can be used to accurately predict the attachment boundary contours for all cases of practical interest.

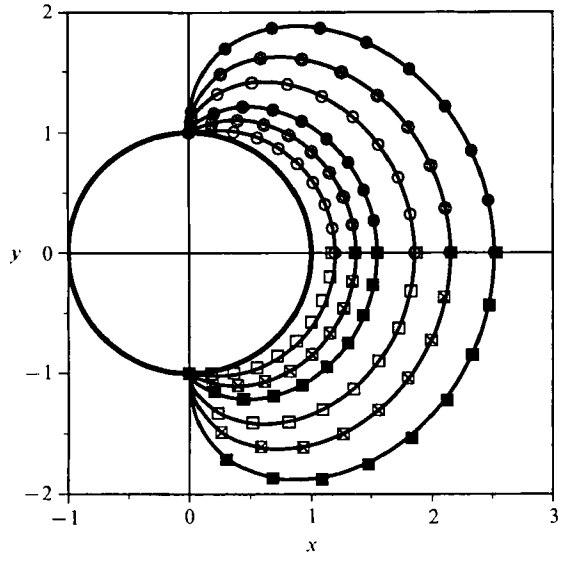

FIGURE 10. The streamline attachment boundary near the pore mouth (solid lines, our numerical results; circles, our asymptotic results using (41); squares, Tutty's (1988). Starting from the centre, these curves correspond to $Q = 2, 5, 10, 25, 50, 100$).

Figure 10 shows our computed attachment boundary contours obtained from the asymptotic expression (41) (circles). These contours cannot be distinguished on the scale shown from our exact results as obtained by means of a numerical integration of $J(R)$ (solid curves). Also plotted in this figure for comparison are Tutty's attachment contours (squares) obtained from his figure 7. It is clear that the agreement is excellent for the entire range $Q \geqslant 2$ and that the neglect of the no-suction shear component, which is included in Tutty's finite-difference solution, is insignificant for these values of Q.

6. Concluding remarks

The results just presented can be applied directly to the blood microcirculation problem described at the beginning of the introduction because the discharge hematocrit H_D and the feed reservoir hematocrit H_F exactly correspond to the respective concentrations C_e and $C_{-\infty}$ used in the last section. In particular, although our analysis has been confined to a greatly simplified geometry and many other factors (e.g. the deformability of the cells and that of the vessel wall, the pulsatile flow condition, the hydrodynamic interaction between the cells in blood, etc.) have been omitted from consideration, the present model does provide the first quantitative theoretical framework for the fluid capture tube which can be used to elucidate phenomena related to the discharge hematocrit defect. For example, the classic experiment by Cokelet (1976), also cited by Chien *et al.* (1984) in their figure 15, revealed that the ratio of H_D/H_F is dependent not only on the size of the cell relative to the pore diamcter, but also on the flow rate in the small tube. Specifically, it was found that in a glass tube 8 μm in diameter, the value of H_D/H_F increased from 0.32 to 0.53 when the mean red cell velocity increased from 8 μm/s to 800 μm/s. In this experiment, the feed reservoir was kept well mixed by a magnetic stirrer, which created a shear flow at the entrance to the glass tube that can be modelled by the flow

geometry in the present paper. The same qualitative dependence of the discharge concentration on the suction flow rate was also observed by Gaehtgens & Papenfuss (1979), whose results are also cited by Chien *et al.* (1984) in their figure 16. In this experiment, a suspension of blood cells was perfused through a cylindrical feed channel (with a diameter of 1.5 mm) at a constant perfusion rate of 30 mm^3/s. When the suction rate through a capillary side branch (diameter = 6.3 μm) was altered from 0 to 10^{-4} mm^3/s, the value of H_D/H_F was observed to increase from 0 to about 0.3. It was also observed by Gaehtgens & Papenfuss (1979) that, when the flow in the feed channel was stopped, H_D/H_F became virtually independent of the suction flow. Surprisingly, little attention was paid in the past to the fact that although the only real difference between this experiment and that of Cokelet was that in the latter the feed reservoir was stirred, yet the results were so different. In general, the dependence of the hematocrit discharge defect on the suction flow rate has been attributed to the enhanced cell deformation at high shear rate, which, as pointed out by Chien *et al.* (1984), reduces the effective size of the cells. Our studies show, however, that cell deformation is not the only determining factor, because figure 13 indicates that, even for rigid spheres, the same trend holds true owing to the dependence of the fluid and particle capture tube shapes on the suction flux into the pore. Moreover, our theory is also consistent with the experimental finding by Gaehtgens & Papenfuss (1979) according to which, in the absence of flow in the feed channel and any stirring, the value of H_D/H_F was found to be nearly independent of the suction rate through the side branch. In contrast, if the deformation of the cell at the entrance to the pore were the primary mechanism causing the discharge hematocrit defect, then one would expect this defect to decrease with an increase in the suction flow rate due to the increased deformation of the cell. Thus, our theory provides a new explanation for the underlying mechanism that causes the discharge hematocrit defect to vary with the suction flow rate.

Although the present theory can be rigorously applied only to dilute suspensions of spheres in a simple shear flow, experimental studies summarized in our companion biological paper, Yan *et al.* (1991), have revealed that the primary effect of increasing the hematocrit concentration is to decrease the plasma layer thickness near the wall. Thus, if this thickness is known as a function of H_F, the plasma skimming effect on the discharge hematocrit defect at higher values of H_F can be estimated by replacing the rigid sphere radius a in the present theory by the measured plasma layer thickness. A second important correction that is required for analysing *in vivo* data in the microcirculation is that the upstream velocity profile is not a simple shear flow, but a flow that closely resembles a Poiseuille flow in the parent vessel. In Yan *et al.* (1991) it is shown that for the microcirculation *in vivo* the average value of Q, neglecting pulse and vasomotor constriction, is approximately 0.1 and that the present small-Q asymptotic solution can be used as the starting point of an accurate approximate theory to describe the changes in the upstream capture cross-section due to an upstream Poiseuille profile. This modified theory is then applied to eatimate the variation in H_D with Q at hematocrit concentrations typical of *in vivo* conditions using the experimentally measured relationship between cell-free layer thickness and H_F, mentioned above.

As noted at the beginning of this paper, the biological problem described above is just one example of the many applications involving the flow of a suspension under shear past a boundary with small pores or side branches. The difficulty in theoretical treating such problems arises from the complexity of the background flow field as well as the difficulty in determining the hydrodynamic coefficients for the

particle–boundary interaction that is required in order to quantitatively describe the particle screening interaction (cf. Wu *et al.* 1991). In the present paper a simplified mathematical model for the flow field and for the fluid skimming effect has been presented. Comparison with Tutty's exact numerical solution of the flow problem shows that our model yields reasonable results, with much less computational effort, for a wide range of suction flow rates. In addition, for large and small values of Q, useful asymptotic expressions were derived in closed form for the shape of the capture tube cross-section. Finally, the particle concentration defect into the pore was computed and its dependence on the particle size and the suction flow rate was found to be in good qualitative agreement with the experimental results reported in the literature.

It is hoped that our model and formulae will also prove to be of value in examining similar problems in other fields.

This research was supported in part by the National Science Foundation under grant CTS-8803116 and by the State of New York under its Einstein Chair Program. The authors also like to thank Dr H. Lipowsky for his insightful comments at the inception of this study and Professor A. M. J. Davis for providing us, ahead of publication, with his solution pertaining to the simple shear flow past an orifice.

Appendix

Consider the simple shear flow

$$V_x = z, \quad V_z = V_y = 0 \quad \text{for} \quad z \geqslant 0$$

past a plate having a circular hole with its centre at the origin, as in figure 1 but without the stem. The solution derived recently by Davis (1991) is as follows for $z \geqslant 0$:

$$\left.\begin{aligned} V_x &= z + \frac{1}{3\pi}\int_0^\infty \mathrm{e}^{-kz}\left(\frac{\sin k}{k} - \cos k\right)\left(\frac{2}{k} - z\right) J_0(kR)\,\mathrm{d}k \\ &\quad + \frac{z}{3\pi}\left[\int_0^\infty \mathrm{e}^{-kz}\left(\frac{\sin k}{k} - \cos k\right) J_2(kR)\,\mathrm{d}k\right]\cos(2\varphi), \\ V_z &= \frac{2z}{3\pi}\left[\int_0^\infty \mathrm{e}^{-kz}\left(\frac{\sin k}{k} - \cos k\right) J_1(kR)\,\mathrm{d}k\right]\cos\varphi, \\ V_y &= \frac{z}{3\pi}\left[\int_0^\infty \mathrm{e}^{-kz}\left(\frac{\sin k}{k} - \cos k\right) J_2(kR)\,\mathrm{d}k\right]\sin(2\varphi). \end{aligned}\right\} \tag{A 1}$$

It can be shown that their asymptotic forms as $z \to 0$ become
(*a*) $0 \leqslant R < 1$, $z < (1-R)$:

$$\left.\begin{aligned} V_x &= \frac{2}{3\pi}(1-R^2)^{\frac{1}{2}} + O(z), \\ V_z &= \frac{2z}{3\pi}\frac{R}{(1-R^2)^{\frac{1}{2}}}\cos\varphi + O(z^2), \\ V_y &= O(z). \end{aligned}\right\} \tag{A 2}$$

(*b*) $R > 1$, $z < (R-1)$:

$$\left.\begin{aligned} V_x &= z\left\{1+\frac{1}{3\pi}\left[\frac{3}{(R^2-1)^{\frac{1}{2}}}-3\sin^{-1}\left(\frac{1}{R}\right)+\frac{\cos(2\varphi)}{R^2(R^2-1)^{\frac{1}{2}}}\right]\right\}+O(z^2), \\ V_z &= \frac{2}{3\pi}\frac{z^2}{R(R^2-1)^{\frac{3}{2}}}\cos\varphi+O(z^3), \\ V_y &= \frac{1}{3\pi}\frac{z}{R^2(R^2-1)^{\frac{1}{2}}}\sin(2\varphi)+O(z^2). \end{aligned}\right\} \tag{A 3}$$

REFERENCES

CHIEN, S., USAMI, S. & SKALAK, R. 1984 In *Handbook of Physiology – The Cardiovascular System IV*, Ch. 6, pp. 217–49. Bethesda, Md: Am. Physiol. Soc.

COKELET, G. R. 1976 In *Microcirculation* (ed. J. Grayson & W. Zingg, Vol. 1, pp. 9–23. Plenum.

CORNHILL, J. F. & ROACH, M. R. 1976 *Atherosclerosis* **23**, 489.

DAGAN, Z., WEINBAUM, S. & PFEFFER, R. 1982 *J. Fluid Mech.* **115**, 505.

DAVIS, A. M. J. 1991 *Phys. Fluids* A **3**, 478.

GAEHTGENS, P. A. L. & PAPENFUSS, H. D. 1979 *Bibliotheca Anat.* **18**, 53.

HAPPEL, J. & BRENNER, H. 1973 *Low Reynolds Number Hydrodynamics*, 2nd edn. Noordhoff.

LIPOWSKY, H. H. 1986 In *Microcirculatory Technology*, Ch. 12, pp. 161–78. Academic.

MOFFATT, H. K. 1964 *J. Fluid Mech.* **18**, 1.

PRIES, A. R., LEY, K. & GAEHTGENS, P. 1986 *Am. J. Physiol.* **251** (*Heart Circ. Physiol.* 20), H1324.

SAMPSON, R. A. 1891 *Phil. Trans. R. Soc. Lond.* A **182**, 449.

SOBEY, I. J. 1977 *J. Fluid Mech.* **83**, 33.

TAKEMUTUSU, M. 1966 *J. Phys. Soc. Japan* **21**, 1816.

TUTTY, O. R. 1988 *J. Fluid Mech.* **191**, 79.

WEINBAUM, S. 1968 *J. Fluid Mech.* **33**, 38.

WU, W. Y., WEINBAUM, S. & ACRIVOS, A. 1991 The motion of a sphere in a shear flow with suction past a plane wall with a hole and its application to particle screening (in preparation).

YAN, Z., ACRIVOS, A. & WEINBAUM, S. 1991 A three-dimensional analysis of plasma skimming and cell screening at microvascular bifurcations. *Microvascular Res.* (in press).